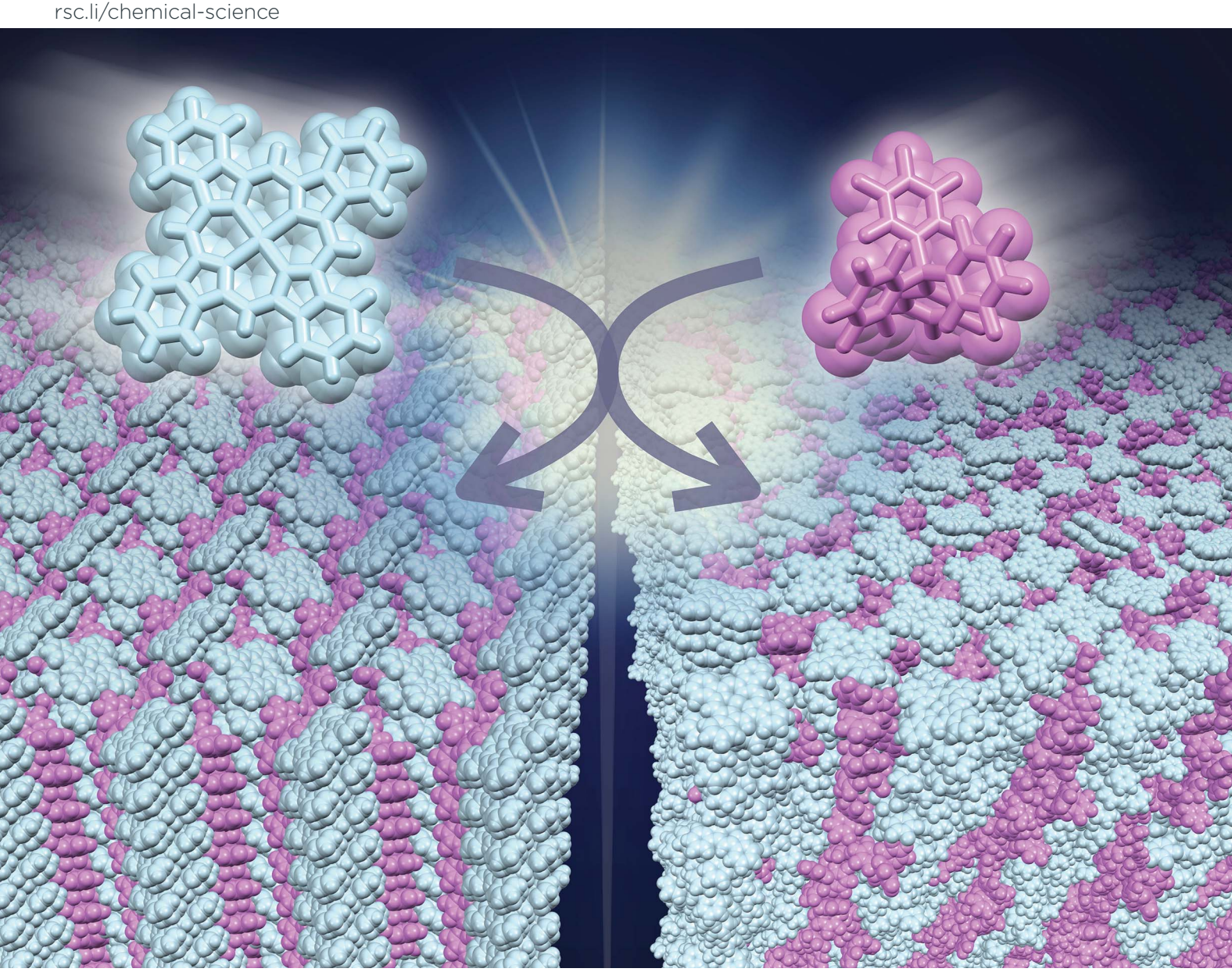
Volume 16 Number 12 28 March 2025 Pages 4903-5312

Chemical Science



ISSN 2041-6539



EDGE ARTICLE

Hiromitsu Maeda *et al.* Electrically conductive charge-segregated pseudo-polymorphs comprising highly planar expanded π -electronic cations



Chemical Science



EDGE ARTICLE

View Article Online
View Journal | View Issue



Cite this: Chem. Sci., 2025, 16, 4998

dll publication charges for this article have been paid for by the Royal Society of Chemistry

Received 8th November 2024 Accepted 6th February 2025

DOI: 10.1039/d4sc07576e

rsc.li/chemical-science

Electrically conductive charge-segregated pseudo-polymorphs comprising highly planar expanded π -electronic cations†

Yohei Haketa, Da Ryoya Nakajima, Yuto Maruyama, Hiroki Tanaka, Wookjin Choi, Shu Seki, Db Shunsuke Sato, Dc Hitomi Baba, Yoshiki Ishii, Dd Go Watanabe, Cd Kirill Bulgarevich, De Kazuo Takimiya, Def Kenzo Deguchi, Shinobu Ohki, Kenjiro Hashi, Takashi Nakanishi, Dj Yukihide Ishibashi, Kazuohika Ohta Dl and Hiromitsu Maeda D**

Independently stacked positively and negatively charged π -electronic systems in charge-segregated columnar structures are desired for electronic properties derived from their electron-deficient and -rich assembling states, respectively. An expanded π -electronic cation, benzoporphyrin Au^{III} complex, was synthesized as the component of ion pairs in combination with counteranions. In contrast to benzoporphyrin, which is known for its insolubility in organic solvents, the ion pairs with bulky anions in this study are soluble in common organic solvents. The ion pairs formed charge-segregated assemblies as two pseudo-polymorphs of single-crystal and less-crystalline (LeC) states based on the stacking of the benzoporphyrin Au^{III} complex. XRD and solid-state NMR measurements, along with molecular dynamics (MD) simulation, revealed that the LeC states were formed by a less-ordered arrangement of constituting ions induced by bulky counteranions. The electric conductivity properties were observed in the single-crystal and LeC charge-segregated assemblies.

^aDepartment of Applied Chemistry, College of Life Sciences, Ritsumeikan University, Kusatsu 525-8577, Japan. E-mail: maedahir@ph.ritsumei.ac.jp

*Advanced Institute for Materials Research (AIMR), Tohoku University, Sendai 980-8577, Japan

^hResearch Network and Facility Services Division, National Institute for Materials Science (NIMS), Tsukuba 305-0003, Japan

'Center for Basic Research on Materials, National Institute for Materials Science (NIMS), Tsukuba 305-0003, Japan

Research Center for Materials Nanoarchitectonics (MANA), National Institute for Materials Science (NIMS), Tsukuba 305-0044, Japan

*Department of Applied Chemistry, Graduate School of Science and Engineering, Ehime University, Matsuyama 790-8577, Japan

Interdisciplinary Graduate School of Science and Technology, Shinshu University, Ueda 386-8567, Japan

† Electronic supplementary information (ESI) available: Synthetic procedures, analytical data, computational details and CIF files for the single-crystal X-ray structural analysis. CCDC 2387040-2387044. For ESI and crystallographic data in CIF or other electronic format see DOI: https://doi.org/10.1039/d4sc07576e

Introduction

The ordered arrangement of π -electronic systems is crucial for charge-carrier transport properties. Expanded π -planes are adequate for achieving high performance in organic semiconductive materials.19 Since substituents affect the electronic states of molecules and their arrangement, π -electronic systems that have no substituents are in great demand.1e However, such systems have low solubility (high crystallinity), making it difficult to arrange the constituents to form assembled structures (Fig. 1a top left). A promising strategy is the preparation of ion pairs of charged π -electronic systems by combining them with counterions that improve solubility (Fig. 1a top right).2 An appropriate combination of charged constituents enables facile handling of π -electronic systems to form counterion-dependent assemblies for applications (Fig. 1a bottom). In particular, independently stacked positively and negatively charged π electronic systems are fascinating because of their ability to form electron-deficient and -rich assembling states, which can function as n- and p-type semiconductive pathways, respectively, in charge-segregated columnar structures. Expanded π systems contribute to influential dispersion forces that overcome electrostatic repulsion in charged columns. The potential positively charged π -systems are porphyrin Au^{III} complexes, which have been included in various ion-pairing assemblies in the form of crystals, supramolecular gels and liquid crystals

^bDepartment of Molecular Engineering, Graduate School of Engineering, Kyoto University, Kyoto 615-8510, Japan

Department of Physics, Graduate School of Science, Kitasato University, Sagamihara 252-0373, Japan

^aDepartment of Data Science, School of Frontier Engineering, Kitasato University, Sagamihara 252-0373. Japan

^eCenter for Emergent Matter Science (CEMS), RIKEN, Wako 351-0198, Japan

Department of Chemistry, Graduate School of Science, Tohoku University, Sendai 980-8578, Japan

Edge Article

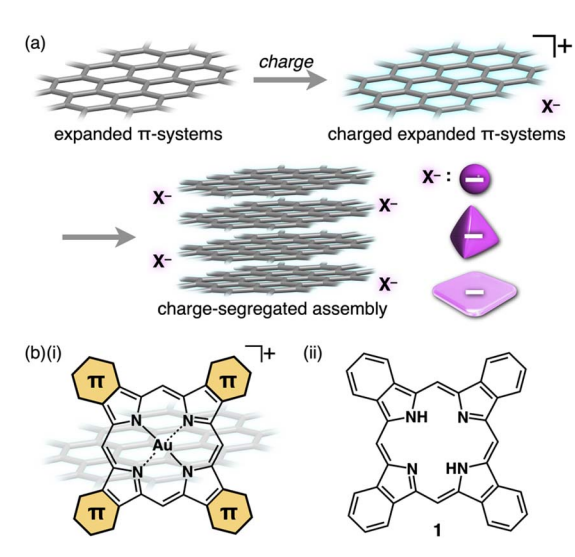


Fig. 1 (a) Expanded π -electronic systems that have no peripheral substituents (top left) and their charged and ion-pairing states (top right, represented as cations), forming a charge-segregated assembly by stacking (bottom) and (b) (i) π -expanded porphyrin Au^{III} complexes as expanded π -electronic cations that can be used in (a) and (ii) benzoporphyrin 1. The positive signs were omitted in the chargesegregated assembly in (a).

depending on the substituents.^{4,5} Expansion of π -electronic systems can be achieved by modifications at the pyrrole βpositions (Fig. 1b(i)). Numerous porphyrin derivatives that have been synthesized to date offered the choice to use benzoporphyrin⁶ 1 (Fig. 1b(ii)) as a framework to provide highly planar charged expanded π-electronic systems. Large planes of benzoporphyrin-based cations are suitable for stacking to form charge-segregated assemblies, whose packing structures can be controlled by coexisting counteranions. The arrangement of substituent-free planar cations and bulky anions can be modulated by crystallization conditions. This study shows π expanded cation-based ion-pairing assemblies in single-crystal and pseudo-polymorph less-crystalline (LeC) states and their electric conductivity properties derived from the chargesegregated assemblies.

Results and discussion

Synthesis and characterization of expanded π -electronic cations

Benzoporphyrins, including metal complexes, can be synthesized from bicyclo[2.2.2]octadiene precursors via retro-Diels-Alder reactions. of In this study, AuIII complexation was conducted for bicycloporphyrin 2 to afford the Au^{III} complex 2au⁺ mainly as a triflate (OTf⁻) ion pair by treatment with KAuCl₄ in the presence of AgOTf and NaOAc (Fig. 2 top). The ion pair 2au⁺-OTf was converted to the Cl ion pair 2au -Cl in 28% yield (two steps) using an ion-exchange resin (Amberlite: IRA402BL Cl). As the selection of the counteranions was crucial in this study, the ion-pair metathesis of $2au^+$ -Cl with AgPF₆, $LiB(C_6F_5)_4$ (LiFABA), $NaB(3,5-(CF_3)_2C_6H_3)_4$ (NaBArF) and NaPCCp (PCCp⁻: pentacyanocyclopentadienide)⁷ afforded the

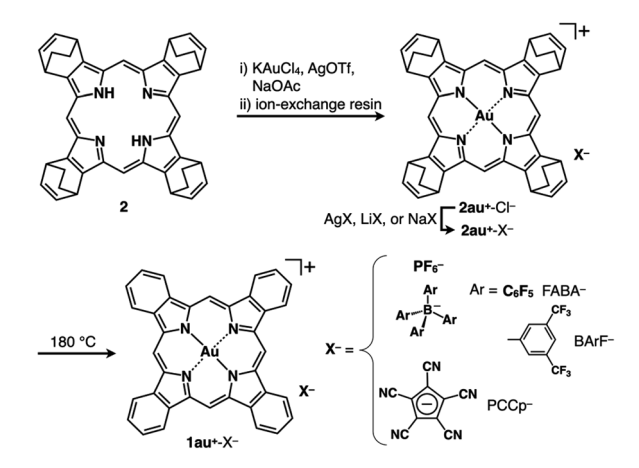


Fig. 2 Synthesis of benzoporphyrin Au^{III} complex ion pairs 1au⁺-X⁻ $(X^- = PF_6^-, FABA^-, BArF^- and PCCp^-)$ via the corresponding bicycloporphyrin Au^{III} complex ion pairs **2au**⁺-X⁻.

corresponding ion pairs $2au^+-X^-(X^- = PF_6^-, FABA^-, BArF^-)$ and PCCp⁻) in 66-76% yields. The obtained ion pairs were characterized by 1H, 13C and 19F NMR and ESI-TOF-MS. DMSO solutions of 2au⁺ ion pairs (4 μM) exhibited Soret and Q-bands at 392 and 507/542 nm, respectively, indicating that 2au⁺ exists as a monomeric state with a negligible counteranion effect on the electronic properties of 2au⁺ (Fig. S12†).8 2au⁺-FABA⁻ and 2au⁺-BArF were also characterized by X-ray analysis for single crystals prepared by vapour diffusion from CH₃CN/water (Fig. 3, S18 and S19†). In the solid-state structures, the cation 2au⁺, refined as one of the stereoisomers, formed stacked dimers with stacking/Au···Au distances of 3.56/3.41 and 3.48/3.37 Å, respectively, and a rotation of $\sim 45^{\circ}$ owing to dispersion forces

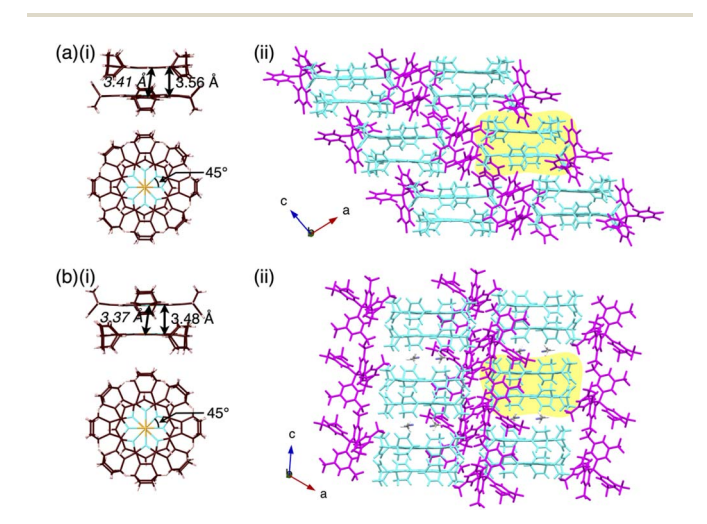


Fig. 3 Single-crystal X-ray structures of (a) 2au⁺-FABA⁻ and (b) 2au⁺-BArF⁻: (i) side and top views of stacked dimers with stacking and Au··· Au (italic) distances and (ii) packing structures with the yellow parts corresponding to the stacked dimers in (i). Atom colour codes in (i): brown, pink, blue and orange refer to carbon, hydrogen, nitrogen and gold, respectively. Colour codes in (ii): cyan and magenta refer to cation and anion parts, respectively. Solvent molecules are omitted in (a), whereas CH₃CN molecules are shown in (b).

at the core planes and β-bicyclo units (Fig. 3a and b(i)). The stacking of 2au⁺ is visualized by Hirshfeld surface analysis, which shows a bow-tie arrangement of red and blue triangles in the shape-index property and flat regions in the curvedness property (Fig. S24 and S25†). Mean-plane deviations of 0.052/ 0.068 and 0.036 Å for stacking 2au⁺ planes (core 25 atoms), respectively, indicate slightly curved 2au⁺ planes, owing to the Au...Au distances being less than the stacking distances. Such remarkably close Au···Au distances are also ascribable to the orbital interactions arising from overlap of the 5dz2 and 6pz orbitals of the adjacent Au^{III}. The stacked 2au⁺ dimers in ion pairs are aligned along the *c*-axis with an offset, which is smaller in 2au+BArF with a longer distance between the stacked dimers by including two CH₃CN molecules (Fig. 3a and b(ii)). In either case, counteranions are located at the side of the stacked 2au⁺ dimers. In particular, BArF⁻ anions are located proximally at the side of the stacked 2au⁺ dimers, forming a pseudohexagonally arranged packing structure along the c-axis (Fig. S19a†).

Stacking of 2au⁺ by overcoming electrostatic repulsion was also observed in the solution state. In CD₃CN, the ¹H NMR of 2au⁺-FABA⁻ showed broad signals at 9.96, 8.37/6.94, 5.98 and 3.49-1.30 ppm ascribable to meso-CH, bicyclo-sp²-CH, bicyclobridged methine-CH and bicyclo-sp3-CH, respectively, for the stacked dimer.11 Concentration-dependent UV/vis absorption spectra of $2au^+$ -FABA⁻ in CH₃CN exhibited a blue shift of λ_{max} from 389 to 374 nm when increasing the concentration from 1.0 imes 10⁻⁶ to 1.0 imes 10⁻⁵ M, suggesting the formation of an H-like stacked dimer at the higher concentration (Fig. S71†). The transition dipole moments of 2au⁺ in the optimized structure of the stacked dimer 2au+2 based on PCM-GD3BJ-B3LYP/6-31+G(d,p) with LanL2DZ for Au (CH₃CN) are arranged at \sim 45°, suggesting that the H-like stacking mode induces a blue shift (Fig. S61a†).12 In addition, TD-DFT calculation of the optimized 2au⁺₂ revealed an absorption at 375 nm, which is blue-shifted by 16 nm compared to the monomer state (Fig. S46†).

According to the synthetic procedure for benzoporphyrin 1,6f $2au^{+}-X^{-}(X^{-}=PF_{6}^{-}, FABA^{-}, BArF^{-} and PCCp^{-})$ were quantitatively transformed to the corresponding benzoporphyrin ion pairs 1au⁺-X⁻ by heating at 180 °C for 20–60 min in the absence of solvent (Fig. 2 bottom). In contrast to 1,6 which is insoluble in most organic solvents, the obtained 1au+X showed enhanced solubility. For example, 1au+FABA was soluble in acetone, DMF, CH3CN and DMSO. In contrast, another ion pair 1au⁺-Cl⁻, which was synthesized from 2au⁺-Cl⁻, was not soluble in these solvents. 13 It is noteworthy that 1au is soluble with facile handling in the form of the ion pairs with appropriate counteranions, although the optimized structure of 1au+ estimated at B3LYP/6-31+G(d,p) with LanL2DZ for Au¹² exhibits completely planar geometry with a mean-plane deviation of 0.00 Å (Fig. S29†). ¹H NMR of $1au^+$ -FABA⁻ in DMSO- d_6 (1.0 mM), as an example, at r.t. exhibited broad signals at 10.21, 9.18 and 8.11 ppm, suggesting soluble but aggregated structures as also indicated by concentration-dependent ¹H NMR (Fig. S74†). ¹⁴ Such ¹H NMR signals in the downfield region suggested the aromatic ring current effect of 1au⁺, which was further supported by nucleus-independent chemical shift (NICS) and the anisotropy of the current induced density (ACID) calculations

(Fig. S54 and S55†). Interestingly, ¹⁹F NMR in the same solvent shows sharp signals derived from FABA⁻ in the dispersed state. The UV/vis absorption spectrum of 1au+FABA in DMSO (4 μM), as a monomer state, exhibits Soret and Q bands of 408 and 564/616 nm, respectively (Fig. 4a), which are more red-shifted than those of 2au+FABA-. The TD-DFT-based UV/vis absorption stick spectrum of 1au⁺ in DMSO shows that these absorptions are mainly derived from the HOMO-1-to-LUMO+1 and HOMO-to-LUMO+1 transitions, respectively (Fig. 4a inset, S49†).

The ¹H NMR of 1au⁺-FABA⁻ in CD₃CN (1.0 mM) shows broader signals than those in DMSO-d₆, suggesting more aggregated structures in the less polar solvent (Fig. S9†). Similar to $2au^+$ -FABA⁻, $1au^+$ -FABA⁻ shows a λ_{max} blue-shift from 402 to 384 nm upon increasing the concentration from 1.8×10^{-7} to 2.0×10^{-5} M in CH₃CN, suggesting the formation of H-like stacked structures (Fig. 4b(i) and S72†). Such a blue shift of the λ_{max} is also observed in variable-temperature (VT)-UV/vis absorption spectra at lower temperatures (Fig. 4b(ii)). TD-DFT calculation of the optimized structure for the stacked dimer 1au⁺₂ at PCM-B3LYP-GD3BJ/6-31+G(d,p) with LanL2DZ for Au (CH₃CN) suggests a slightly blue-shifted Soret band compared to that of the monomeric state (Fig. S51†). The dimerization constant (K_{dim}) of $1au^+$ for $1au^+$ -FABA⁻ is estimated to be 5 \times

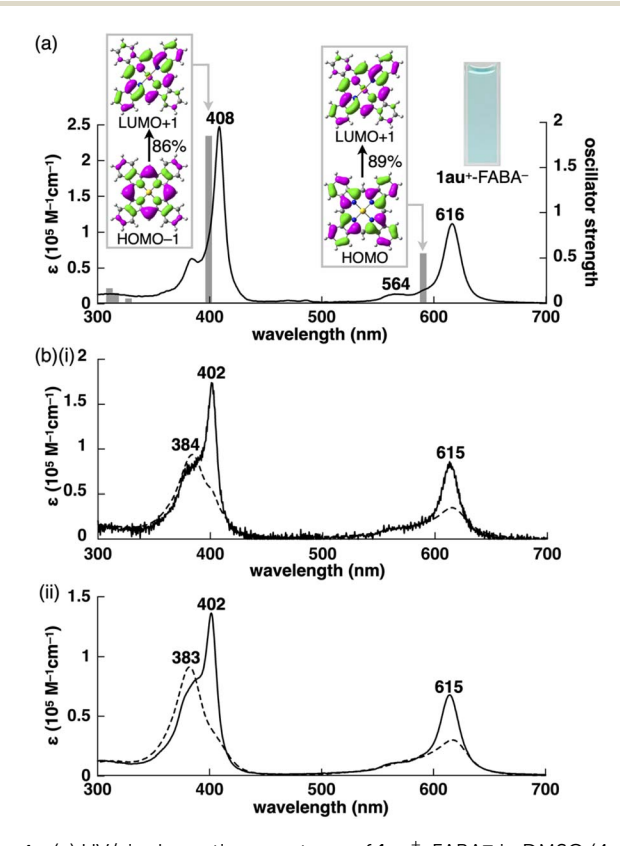


Fig. 4 (a) UV/vis absorption spectrum of $1au^+$ -FABA⁻ in DMSO (4 μ M) (inset: photograph of the DMSO solution (4 μ M)) and TD-DFT-based UV/vis absorption stick spectrum (grey bar) of 1au⁺ at PCM-B3LYP-GD3BJ/6-31+G(d,p) with LanL2DZ for Au (DMSO) and (b) UV/vis absorption spectra of **1au**⁺-FABA⁻ in CH₃CN according to (i) concentrations (solid line: 0.18 µM and broken line: 20 µM) and (ii) temperatures (solid line: 70 °C and broken line: -40 °C).

Edge Article Chemical Science

 $10^6~M^{-1}$ in CH_3CN at r.t. from concentration-dependent UV/vis absorption spectral changes (Fig. S72†). $\pi\textsc{-}Expansion$ of positively charged $\pi\textsc{-}electronic$ systems induces influential dispersion forces, which enable the stacking of identically charged $\pi\textsc{-}electronic$ systems.

Single-crystal-state charge-segregated assemblies

Prism-shaped single crystals of the ion pairs $1au^+X^-$ (X^- = FABA $^-$, BArF $^-$ and PCCp $^-$), obtained from CH₃CN/CHCl₃,¹⁵ 1,1,1-trichloroethane/n-heptane and DMF/o-dichlorobenzene, respectively, were suitable for X-ray analysis, revealing the exact structures of the ion pairs and their assembled structures (Fig. 5). In these structures, the cation $1au^+$, showing planar geometry with mean-plane deviations (core 25 atoms) of 0.016, 0.031/0.011 and 0.023 Å, respectively, forms closely stacked columnar structures with stacking distances of 3.29, 3.36/3.44 and 3.37 Å, respectively, in the charge-segregated mode (Fig. 5a-c(i)). The stacked parts of $1au^+$ are clearly shown by Hirshfeld surface analysis, exhibiting a bow-tie arrangement of red and blue triangles in the shape-index property and flat regions in the curvedness property (Fig. S26–S28†). The Au···Au

distances are 4.76, 3.93/4.59 and 3.81 Å, respectively, suggesting that the offset stacking of the cations is larger for **1au**⁺-FABA⁻. The angles of 44.1°, 48.4°/60.1° and 62.1° are estimated, respectively, for the lines passing through two Au atoms of stacked 1au⁺ to the corresponding 41-atom mean planes. In these ion pairs, counteranions FABA⁻, BArF⁻ and PCCp⁻ are located at the side of the columnar structures (Fig. 5a-c(ii) and (iii)). The ion-pair crystals $1au^+$ -FABA $^-$, $1au^+$ -BArF $^-$ and $1au^+$ -PCCp formed orthorhombic, monoclinic and orthorhombic packing, respectively, with the columns of stacked 1au+ aligned along the a-, c- and a-axes, respectively, which are the long axes of the prism crystals (Fig. S23†). Notably, the stacked 1au⁺ in the columns are tilted, with angles of 30.4°, 2.9°/3.0° and 21.2°, respectively, relative to the stacking axis (Fig. 5a-c(ii)). Interestingly, in the crystal packing of **1au**+FABA, an ion-pair framework composed of columnar cation structures and counteranions forms two tubular spaces per unit cell, with a volume of 5.56 nm³, containing disordered solvent molecules. The solvent molecules in the single crystal are not removed after heating at 100 °C under vacuum, as revealed by the X-ray analysis.

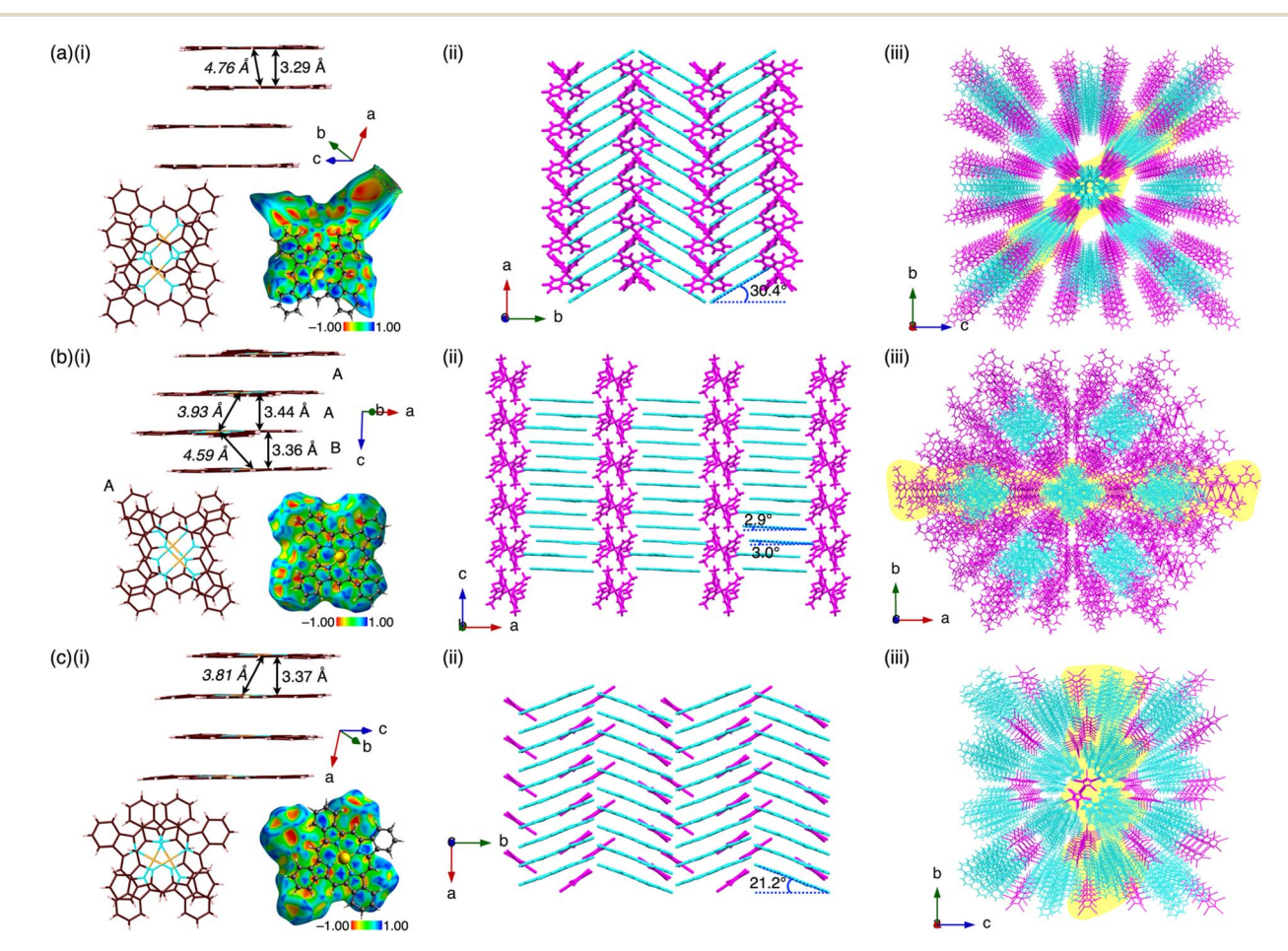


Fig. 5 Single-crystal X-ray structures of (a) $1au^+$ -FABA⁻, (b) $1au^+$ -BArF⁻ and (c) $1au^+$ -PCCp⁻: (i) side views of the columnar structures of stacked $1au^+$ with stacking and Au···Au (italic) distances and top views along with Hirshfeld surface mapped over the shape-index property of the stacked dimer, (ii) packing structures of columns of stacked $1au^+$ and counteranions and (iii) packing structures with the yellow parts corresponding to the packing structures in (ii). In (b), the different types of stacking arrangements are indicated by A and B (stacking arrangement A is shown as a representative). Atom colour codes in (i): brown, pink, blue and orange refer to carbon, hydrogen, nitrogen and gold, respectively. Colour codes in (ii): cyan and magenta refer to cation and anion parts, respectively.

Chemical Science Edge Article

To evaluate the stacking behaviour of $\mathbf{1au}^+$ in the crystal structures, energy decomposition analysis (EDA)^{16,17} was performed using the fragment molecular orbital (FMO) method (FMO2-MP2) with mixed basis sets including NOSeC-V-DZP with MCP with NOSeC-V-TZP with MCP for $\mathbf{Au}^{18,19}$ The EDA calculations using FMO yielded $E_{\rm es}$, $E_{\rm disp}$, $E_{\rm ct}$ and $E_{\rm ex}$ (energies for electrostatic, dispersion, charge-transfer forces and exchange repulsion, respectively) and $E_{\rm tot}$ (total energy). In the columnar structure of $\mathbf{1au}^+$ in $\mathbf{1au}^+$ -FABA $^-$, an $E_{\rm tot}$ of -164.2 kcal mol^{-1} is observed, whereas $E_{\rm disp}$ and $E_{\rm es}$ are -214.0 and 6.5 kcal mol^{-1} , respectively, indicating that $E_{\rm disp}$ is a major force in the stacking structure (Fig. 6 and S58†). EDA calculations for $\mathbf{1au}^+$ -BArF $^-$ and $\mathbf{1au}^+$ -PCCp $^-$ also elucidated similar energy balances for neighbouring π -electronic ions (Fig. S59 and S60†).

Crystal-state absorptions of the ion pairs 1au⁺-FABA⁻, 1au⁺-BArF⁻ and **1au**⁺-PCCp⁻ were evaluated *via* optical microscopy for spectroscopic examination (Fig. S75 and S76†). In 1au⁺-FABA⁻, the absorptions at 587 and 623 nm, which are slightly blue- and red-shifted, respectively, compared to those of the monomer in DMSO (616 nm), are ascribable to the exciton coupling in a predominantly J-like arrangement and also very weak coupling for orthogonally arranged transition dipole moments (Fig. 7 and S62†). These behaviours are derived from the D_{4h} geometry of $1au^+$. Similar to $1au^+$ -FABA⁻, the crystalstate absorption of 1au⁺-PCCp⁻ shows absorptions at 588 and 623 nm, which are ascribable to the exciton coupling of stacked 1au⁺. On the other hand, 1au⁺-BArF⁻ mainly exhibits a blueshifted broad absorption at 585 nm with a shoulder at 654 nm. The blue-shifted absorption can be attributed to the larger contribution of the H-like arrangement of transition dipoles in the stacked **1au**⁺ (Fig. S62†).

Charge-segregated assemblies of π -electronic ion pairs show fascinating electric conductivity properties. The electric conductivity properties of stacked $1au^+$ in the ion pairs $(1au^+FABA^-, 1au^+BArF^-$ and $1au^+PCCp^-)$ were evaluated by flash-photolysis time-resolved microwave conductivity (FP-TRMC) measurements (Fig. 8a and S91†). Electric conductivity $(\phi \Sigma \mu)$ values of 4.6×10^{-9} , 9.2×10^{-9} and 2.9×10^{-9} m 2 V $^{-1}$ s $^{-1}$ were

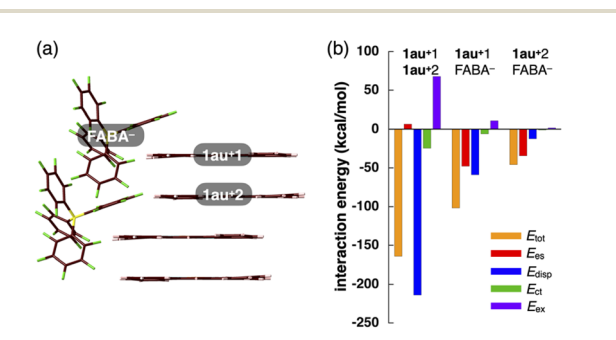


Fig. 6 Decomposition of the total intermolecular interaction energies (E_{tot}) of $\mathbf{1au}^+$ -FABA $^-$ for (a) the single-crystal X-ray structure and (b) estimated interaction energies (kcal mol $^{-1}$) according to EDA based on the FMO2-MP2 method using a basis set of NOSeC-V-DZP with MCP with NOSeC-V-TZP with MCP for Au (see Table S4† for the complete data list). Colour codes in (i): brown, pink, blue, yellow, green and orange refer to carbon, hydrogen, nitrogen, boron, fluorine and gold, respectively.

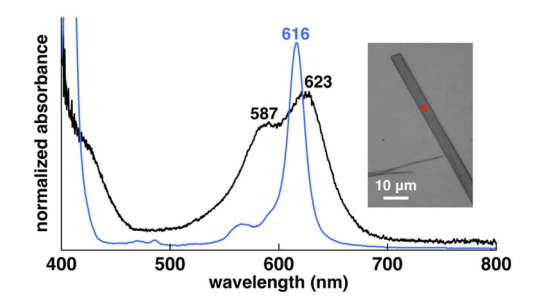


Fig. 7 Solid-state UV/vis absorption spectra of $1au^+$ -FABA $^-$ in the single crystal (black line) and in DMSO (4 μ M) (blue line) as a reference (inset: photograph of the single crystal (red circle indicates the position of measurement)).

observed for the longer axes of the respective single crystals. Clear anisotropic electric conductivity was shown in 1au⁺-BArF⁻ $(7.9 \times 10^{-9} \text{ m}^2 \text{ V}^{-1} \text{ s}^{-1} \text{ for the shorter axis})$. These values are comparable to and greater than those of previously reported charge-segregated assemblies.³ The order of the $\phi \Sigma \mu$ values, 1au⁺-BArF⁻ > 1au⁺-FABA⁻ > 1au⁺-PCCp⁻, is consistent with the theoretically estimated transfer integrals t at PW91/TZP for the stacked 1au⁺ units in the crystal structures, showing hole transfer integrals $|t|_h$ of 118.5/50.5, 21.3 and 9.8 meV, respectively (Fig. 8b and S63†).21 Furthermore, theoretically estimated HOMO band dispersions using the tight-binding approximation²² for the stacked 1au⁺ in the single-crystal structures of 1au⁺-FABA⁻, 1au⁺-BArF⁻ and 1au⁺-PCCp⁻ exhibited onedimensional band structures, which are consistent with the stacking structures of 1au⁺ (Fig. S64†). The Fermi levels lie in the middle of the band gaps, suggesting that charge-segregated assemblies comprising stacked 1au+ exhibit semiconductive behaviours. In the discussed ion pairs, decreased on-site Coulomb repulsion between stacked π -electronic cations with expanded π -electronic systems would induce hole transport rather than electron transport. The conductivity transients

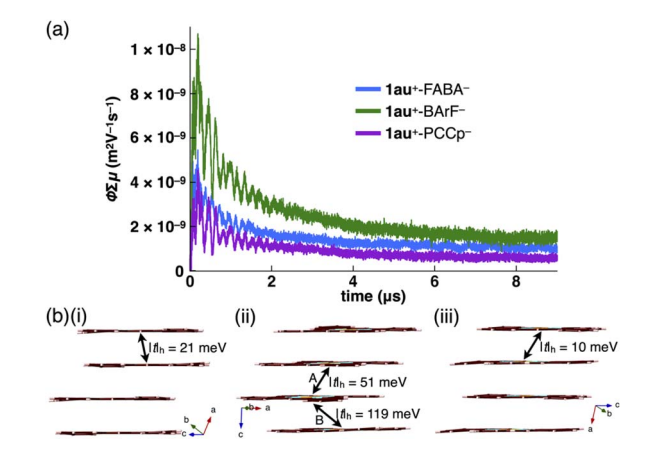


Fig. 8 (a) Photoconductivity transients observed upon excitation at 355 nm, 9.1×10^{15} photons per cm² per pulse, for the long axis of the single crystals of $1au^+$ -FABA $^-$ (blue), $1au^+$ -BAFF $^-$ (green) and $1au^+$ -PCCp $^-$ (purple) and (b) stacked $1au^+$ in the single crystal structures of (i) $1au^+$ -FABA $^-$, (ii) $1au^+$ -BAFF $^-$ and (iii) $1au^+$ -PCCp $^-$ and hole transfer integrals ($|t|_h$) estimated at PW91/TZP. Stacking modes A and B in (ii) correspond to Fig. 5b(i).

recorded under an SF₆ atmosphere with negligible quenching of charge carriers suggest a major contribution from holes photoinjected into the assemblies (Fig. S92†).23

Charge-segregated assemblies in pseudo-polymorph lesscrystalline states

Substituent-free benzoporphyrins in the forms of free base and metal complexes have been known to show highly crystalline states after heating the corresponding bicyclo[2.2.2]octadiene precursors in the film state. 6h In contrast, 1au as ion pairs can form bulk materials that are not single crystals via recrystallization from appropriate solvents. Precipitation of 1au⁺-FABA⁻ from acetone/n-hexane provided a material (labelled as 1au+ FABA_P) that appeared to differ from the single crystals (Fig. 9a inset).24 The synchrotron XRD of 1au+FABA at 25 °C exhibited broad peaks instead of crystalline diffraction, suggesting the formation of an LeC state for the obtained precipitates. The diffraction peaks of 1.81, 1.04, 0.90, 0.68, 0.60, 0.52, 0.50, 0.45, 0.41 and 0.34 nm, showing Debye-Scherrer rings, were assigned to the hkl parameters derived from a hexagonal pattern (100, 110, 200, 210, 300, 220, 310, 400 and 320) as a = 2.09 nm (Fig. 9a and S81†).25 The intense peak at 0.34 nm was assigned to 001 as the stacking distance of 1au⁺ in the hexagonal columnar (Col_h) structure (Z = 1 for $\rho = 1.79$ g cm⁻³) (Fig. 9b). Interestingly, heating the powder sample of 2au⁺-FABA^{- 26} at 190 °C (labelled as 1au⁺-FABA⁻_H) also formed a Col_h structure identical to that of 1au⁺-FABA⁻_P (Fig. S79–S82[†]). In contrast to the tilted 1au⁺ plane along the a-axis in the single crystal of 1au⁺-FABA⁻, the 1au⁺ plane in 1au⁺-FABA⁻_P should be arranged perpendicularly to the stacking axis, as indicated by the intracolumnar stacking period of 0.34 nm. On the basis of the Col_h structure with a =2.09 nm and the sizes of **1au**⁺ and FABA⁻, columnar structures comprising less-ordered stacking of 1au⁺, as indicated by cyan circles, are located close to FABA-, as indicated by magenta circles (Fig. 9b(ii)).

The proximal location of **1au**⁺ and FABA⁻ is also suggested by the optimized structure of dimeric 1au⁺-FABA⁻ using B3LYP-GD3BJ/6-31+G(d,p) with LanL2DZ for Au (Fig. 9c). FABA should be paired with several **1au**⁺ in the proximal location, although the XRD pattern suggests that the location of FABA- is less clear, probably indicating an amorphous-like state. In light of the stoichiometry of the constituents and their contrasting planar and bulky shapes, FABA would be observed in three sites on average among the 1au⁺ columns, and, in another cross section according to the 1au⁺ planes, the anions should be located in the other three sites. As a result, FABA can be hexagonally arranged around the 1au⁺ columns. The Col_h structure suggested by the XRD pattern is clearly demonstrated by all-atom molecular dynamics (MD) simulations at 25 °C after 100 ns of the equilibration run (Fig. 9d and S66†). Notably, as the initial structure for the MD simulation, the columns comprising tilted 1au⁺ units, as observed in the single-crystal structure, are transformed to a structure with barely tilted 1au⁺. The combination of planar 1au⁺, suitable for stacking, and bulky FABA⁻, with a less-ordered arrangement via noncovalent interactions induces the LeC state.27,28 The less-ordered FABA

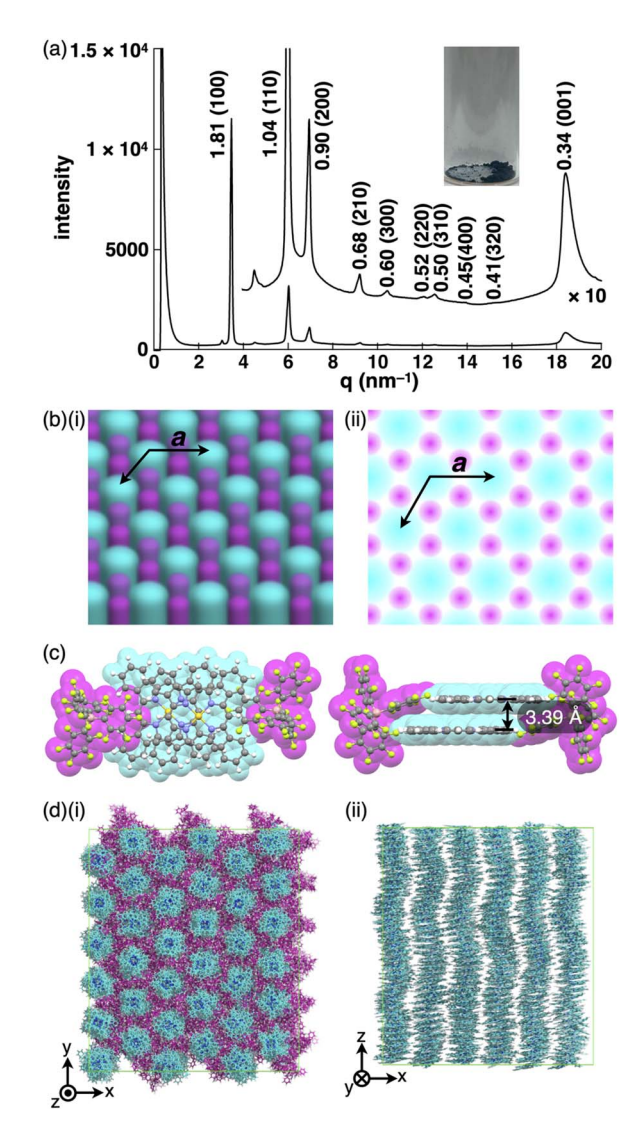


Fig. 9 (a) Synchrotron XRD pattern of 1au⁺-FABA⁻_P at 25 °C for the sample obtained by precipitation from acetone/n-hexane (inset: photograph of the precipitates), (b) schematic representation for the Col_b packing structure: (i) packing diagram and (ii) top view of Col_b (1au⁺ and FABA⁻ are represented in cyan and magenta, respectively), (c) top and side views of the optimized structure of **1au**⁺-FABA⁻ as a dimer using B3LYP-GD3BJ/6-31+G(d,p) with LanL2DZ for Au and (d) snapshot of the MD simulation result for 1au+-FABA-P after 100 ns of the equilibration run at 25 °C showing (i) the top view of the packing diagram and (ii) the side view of 1au+ columns extracted from the packing diagram (1au+ and FABA- are represented in cyan and magenta, respectively). In (b) (ii), magenta circles suggest the possible locations of FABA⁻ with a 50% occupancy rate on average in a cross section, whereas cyan circles show the diameter of 1au⁺ columns in slipped stacking.

interferes with the ordered packing of 1au⁺ for crystallization. 1au⁺-FABA⁻_P maintains the Col_h structure up to 195 °C and is converted to a complicated crystalline state at higher temperatures, with decomposition at 355 °C. This behaviour is also supported by differential scanning calorimetry (DSC) analysis (Fig. S78†). The appearance of **1au**⁺-FABA_P as a dark blue powder in polarized optical microscopy (POM) was maintained through the heating process. The condition-dependent

Chemical Science

assembly (single-crystal and LeC states) as pseudo-polymorphism²⁹ is fascinating for tuneable properties according to the arrangement of building blocks. The Colh LeC state, in the absence of aliphatic chains, is rare²⁸ but can be achieved by pairing the planar π -electronic cation with a bulky counteranion.30

The details of the structures of 1au⁺-FABA⁻ were investigated by solid-state NMR (SSNMR) spectroscopy. ¹³C NMR was performed using cross-polarization magic-angle spinning (CPMAS) (Fig. 10 and S86†). Dipolar dephasing experiments were conducted to support the signal assignment for the ion pair (Fig. S86 and S88†). The broad signals at 132.2, 120.8, 93.4 and 89.3 ppm were assigned to 1au⁺, whereas those at 149.7, 137.7 and 126.0 ppm were assigned to FABA⁻ (Fig. 10a). ¹³C CPMAS NMR of 1au⁺-FABA⁻_H showed slightly broader signals than 1au⁺-FABA⁻_P, suggesting the formation of a more disordered arrangement of constituting ions (Fig. 10b). In contrast, ¹³C CPMAS NMR for 1au⁺-FABA⁻ as single crystals showed narrower signals than those of $1au^+$ -FABA $^-$ _P and $1au^+$ -FABA $^-$ _H (Fig. 10c), suggesting that the broader signals of 1au⁺-FABA_P and 1au⁺-FABA H indicated a less-ordered arrangement of ions that form Col_h structures. Similar signal broadening was observed for ¹⁹F and ¹¹B MAS NMR of **1au**⁺-FABA⁻_P and **1au**⁺-FABA⁻_H (Fig. S89 and S90†). Moreover, the characteristic up-field split signals at 93.4 and 89.3 ppm in 1au⁺-FABA⁻_P are derived from unsubstituted meso-carbons,31 as also suggested by theoretically estimated NMR signals for 1au⁺ using B3LYP/6-311+G(d,p) with SDD for Au (Fig. S65†).12 Such signal splitting is also observed in the ¹³C CPMAS NMR of the single crystals due to slipped stacking of **1au**⁺ observed in the crystal structure of **1au**⁺-FABA⁻ (Fig. 5a(i)).32 These observations, along with the XRD analysis and MD simulation, support a less-ordered slipped stacking structure for **1au**⁺ in a column of Col_h LeC states, wherein the 1au⁺ planes are more perpendicularly arranged to the column compared to those in the single crystal.33

The formation of such an LeC state was also observed in the precipitate of 1au⁺-BArF⁻_P prepared from acetone/n-hexane.³⁴ Similar to 1au⁺-FABA⁻_P, 1au⁺-BArF⁻_P shows a Col_h LeC state (a

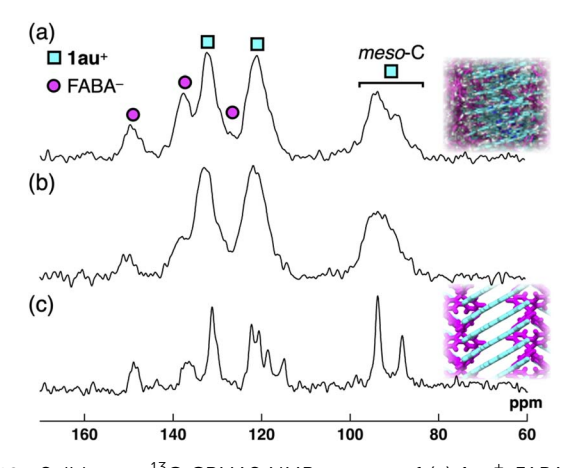


Fig. 10 Solid-state ¹³C CPMAS NMR spectra of (a) 1au⁺-FABA⁻_P, (b) 1au⁺-FABA⁻_H and (c) 1au⁺-FABA⁻ as single crystals recorded at 20 kHz MAS spinning frequency at r.t. with the corresponding packing diagrams

= 2.28 nm, c = 0.34 nm, and Z = 1 for $\rho = 1.71$ g cm⁻³) (Fig. S84 and S85†), also exhibiting condition-dependent pseudopolymorphs. Colh LeC states in the precipitates were observed for 1au+FABA and 1au+BArF, which formed orthorhombic and monoclinic single-crystal packing structures, respectively. Such pseudo-polymorphic phenomena are fascinating because stacking of 1au+ can be easily controlled by the assembly conditions. The electric conductivity $(\phi \Sigma \mu)$ values of LeC-state 1au⁺-FABA⁻_P, 1au⁺-FABA⁻_H and 1au⁺-BArF⁻_P were estimated to be 1.2×10^{-9} , 1.0×10^{-9} and 3.4×10^{-9} m² V⁻¹ s⁻¹, respectively, suggesting that electrically conductive pathways also exist in the columnar structures of LeC materials, although the values are smaller than those of the corresponding single crystals (Fig. S93†).

Conclusions

Ion-pairing assemblies in charge-segregated modes were constructed from a highly planar expanded π -electronic cation in combination with counteranions. Charge-segregated assemblies were formed with both planar and bulky counteranions by means of stable stacked structures of the expanded π -electronic cation. The stacking arrangement and resulting absorption spectra in the single crystals were modulated by coexisting anions. Depending on crystallizing solvent conditions, ion pairs with bulky borate anions also provided LeC states as pseudopolymorphs of their single crystals. Both single crystals and LeC states exhibited electric conductive properties due to stacking of the π -expanded porphyrin Au^{III} complex.³⁵ It is noteworthy that the discussed planar π -electronic cation, benzoporphyrin Au^{III} complex, is soluble in organic solvents in the ion-pairing states. Ion pairing is an effective strategy to increase the solubility of planar π -electronic systems for their facile handling and the fabrication of assembled structures with ordered arrangements. Further modifications of charged π electronic systems would lead to ion-pairing assemblies that can be applied for functional electronic materials and devices.

Data availability

Data supporting the work in this publication are available via the ESI and associated crystallographic data.

Author contributions

H. M. designed and conducted the project. Y. H., R. N., Y. M. and H. T. carried out the synthesis, characterization and property examinations. W. C. and S. Se. evaluated the electric conductivities. S. Sa., H. B., Y. I. and G. W. conducted the MD calculations. K. B. and K. T. conducted the transfer integral calculations. K. D., S. O., K. H. and T. N. evaluated the SSNMR. Y. I. and T. A. recorded the solid-state absorption spectra. K. O. supported the discussion on the assemblies.

Conflicts of interest

There are no conflicts of interest to declare.

Acknowledgements

This work was supported by JSPS KAKENHI Grant Numbers JP18H01968, JP22H02067 and JP23K23335 for Scientific Research (B), JP19K05444 and JP24K08389 for Scientific Research (C), JP20J22745 for JSPS Fellows, JP23K17951 for Challenging Research (Exploratory) and JP20H05863 for Transformative Research Areas (A) "Condensed Conjugation", JST SPRING, Grant Number JPMJSP2101 and Ritsumeikan Global Innovation Research Organization (R-GIRO) project (2017–22 and 2022–27). Theoretical calculations were partially performed using the Research Center for Computational Science, Okazaki, Japan (Projects: 20-IMS-C079, 21-IMS-C077, 22-IMS-C077, 23-IMS-C069 and 24-IMS-C067). Synchrotronradiation analysis was performed at BL40XU (2021B1703 and 2022B1149), BL02B1 (2024A1644) and BL40B2 (2021B1828, 2022A1689, 2022B1546, 2023A1331, 2023B1409 and 2024A1463) of SPring-8 with the approval of the Japan Synchrotron Radiation Research Institute (JASRI). A part of this work was supported by "Advanced Research Infrastructure for Materials and Nanotechnology in Japan (ARIM)" of the Ministry of Education, Culture, Sports, Science and Technology (MEXT). We thank Dr Noboru Ohta, JASRI/SPring-8, for synchrotron-XRD measurements, Dr Nobuhiro Yasuda, JASRI/SPring-8 and Prof. Takuji Hatakeyama, Kyoto University, for single-crystal synchrotron-Xray analysis, Prof. Osamu Tsutsumi, Ritsumeikan University, for single-crystal X-ray analysis, Prof. Yasuteru Shigeta, University of Tsukuba, for theoretical study and Prof. Hitoshi Tamiaki, Ritsumeikan University, for various measurements.

Notes and references

- 1 Selected books and reviews on supramolecular assemblies for electronic materials: (a) Functional Supramolecular Architectures: For Organic Electronics and Nanotechnology, ed. P. Samorì and F. Cacialli, Wiley, Weinheim, 2011; (b) Supramolecular Materials for Opto-Electronics, ed. N. Koch, RSC, Cambridge, 2015; (c) T. Wöhrle, I. Wurzbach, J. Kirres, A. Kostidou, N. Kapernaum, J. Litterscheidt, J. C. Haenle, P. Staffeld, A. Baro, F. Giesselmann and S. Laschat, Chem. Rev., 2016, 116, 1139–1241; (d) J. Urieta-Mora, I. García-Benito, A. Molina-Ontoria and N. Martín, Chem. Soc. Rev., 2018, 47, 8541–8571; (e) P. Yu, Y. Zhen, H. Dong and W. Hu, Chem, 2019, 5, 2814–2853; (f) C. J. Kousseff, R. Halaksa, Z. S. Parr and C. B. Nielsen, Chem. Rev., 2022, 122, 4397–4419; (g) J. Chen, W. Zhang, L. Wang and G. Yu, Adv. Mater., 2023, 35, 2210772.
- 2 Y. Haketa, K. Yamasumi and H. Maeda, *Chem. Soc. Rev.*, 2023, 52, 7170–7196.
- 3 (a) K. Yamasumi, K. Ueda, Y. Haketa, Y. Hattori, M. Suda, S. Seki, H. Sakai, T. Hasobe, R. Ikemura, Y. Imai, Y. Ishibashi, T. Asahi, K. Nakamura and H. Maeda, *Angew. Chem., Int. Ed.*, 2023, **62**, e202216013; (b) S. Takahashi, M. Murai, Y. Hattori, S. Seki, T. Yanai and S. Yamaguchi, *J. Am. Chem. Soc.*, 2024, **146**, 22642–22649; (c) K. Yamasumi, H. Horita, Y. Haketa, S. Seki, K. Bulgarevich, K. Takimiya,

- H. Shimogawa and H. Maeda, *Chem.-Eur. J.*, 2025, **31**, e202404781.
- 4 Selected reports of porphyrin Au^{III} complexes: (a) E. B. Fleischer and A. Laszlo, *Inorg. Nucl. Chem. Lett.*, 1969, 5, 373–376; (b) R. Timkovich and A. Tulinsky, *Inorg. Chem.*, 1977, 16, 962–963; (c) M. E. Jamin and R. T. Iwamoto, *Inorg. Chim. Acta*, 1978, 27, 135–143.
- 5 (a) Y. Haketa, Y. Bando, Y. Sasano, H. Tanaka, N. Yasuda,
 I. Hisaki and H. Maeda, iScience, 2019, 14, 241–256; (b)
 H. Tanaka, Y. Kobayashi, K. Furukawa, Y. Okayasu,
 S. Akine, N. Yasuda and H. Maeda, J. Am. Chem. Soc., 2022,
 144, 21710–21718; (c) Y. Maruyama, K. Harano, H. Kanai,
 Y. Ishida, H. Tanaka, S. Sugiura and H. Maeda, Angew.
 Chem., Int. Ed., 2025, 64, e202415135.
- 6 A review and selected reports of benzoporphyrins: (a) C. M. B. Carvalho, T. J. Brocksom and K. T. de Oliveira, Chem. Soc. Rev., 2013, 42, 3302-3317; (b) R. P. Linstead and F. T. Weiss, J. Chem. Soc., 1950, 2975-2981; (c) C. O. Bender, R. Bonnett and R. G. Smith, J. Chem. Soc. C, 1970, 1251-1257; (d) C. O. Bender, R. Bonnett and R. G. Smith, J. Chem. Soc., Perkin Trans. 1, 1972, 6, 771-776; (e) M. G. H. Vicente, A. C. Tomé, A. Walter and A. S. Cavaleiro, Tetrahedron Lett., 1997, 38, 3639-3642; (f) S. Ito, T. Murashima, N. Ono and H. Uno, Chem. Commun., 1998, 1661-1662; (g) P. B. Shea, J. Kanicki, L. R. Pattison, P. Petroff, M. Kawano, H. Yamada and N. Ono, J. Appl. Phys., 2006, 100, 034502; (h) N. Noguchi, S. Junwei, H. Asatani and M. Matsuoka, Cryst. Growth Des., 2010, 10, 1848-1853; (i) K. Takahashi, B. Shan, X. Xu, S. Yang, T. Koganezawa, D. Kuzuhara, N. Aratani, M. Suzuki, Q. Miao and H. Yamada, ACS Appl. Mater. Interfaces, 2017, 9,8211-8218.
- 7 (a) O. W. Webster, J. Am. Chem. Soc., 1965, 87, 1820–1821; (b)
 T. Sakai, S. Seo, J. Matsuoka and Y. Mori, J. Org. Chem., 2013, 78, 10978–10985.
- 8 2au⁺ can be obtained as a single isomer prepared from the separated isomer of 2. Details on the synthetic procedures and properties will be discussed elsewhere.
- 9 P. R. Spackman, M. J. Turner, J. J. McKinnon, S. K. Wolff, D. J. Grimwood, D. Jayatilaka and M. A. Spackman, *J. Appl. Crystallogr.*, 2021, **54**, 1006–1011.
- 10 W. Lu, K. T. Chan, S.-X. Xu, Y. Chen and C.-M. Che, *Chem. Sci.*, 2012, **3**, 752–755.
- 11 The dimerization constant ($K_{\rm dim}$) for $2au^+$ -FABA⁻ was estimated to be $1.1 \times 10^5~{\rm M}^{-1}$ from the monomer/dimer ratio of 1 H NMR signals in ${\rm CD_2Cl_2}$ (5 \times 10⁻⁵ M) at 20 $^{\circ}$ C (Fig. S73†).
- M. J. Frisch, G. W. Trucks, H. B. Schlegel, G. E. Scuseria, M. A. Robb, J. R. Cheeseman, G. Scalmani, V. Barone, G. A. Petersson, H. Nakatsuji, X. Li, M. Caricato, A. V. Marenich, J. Bloino, B. G. Janesko, R. Gomperts, B. Mennucci, H. P. Hratchian, J. V. Ortiz, A. F. Izmaylov, J. L. Sonnenberg, D. Williams-Young, F. Ding, F. Lipparini, F. Egidi, J. Goings, B. Peng, A. Petrone, T. Henderson, D. Ranasinghe, V. G. Zakrzewski, J. Gao, N. Rega, G. Zheng, W. Liang, M. Hada, M. Ehara, K. Toyota, R. Fukuda, J. Hasegawa, M. Ishida, T. Nakajima, Y. Honda,

- O. Kitao, H. Nakai, T. Vreven, K. Throssell, J. A. Montgomery Jr, J. E. Peralta, F. Ogliaro, M. J. Bearpark, J. J. Heyd, E. N. Brothers, K. N. Kudin, V. N. Staroverov, T. A. Keith, R. Kobayashi, J. Normand, K. Raghavachari, A. P. Rendell, J. C. Burant, S. S. Iyengar, J. Tomasi, M. Cossi, J. M. Millam, M. Klene, C. Adamo, R. Cammi, J. W. Ochterski, R. L. Martin, K. Morokuma, O. Farkas, J. B. Foresman and D. J. Fox, *Gaussian 16, Revision C.01*, Gaussian, Inc., Wallingford CT, 2016.
- 13 **1au**⁺ with BArF⁻ was also soluble in CH₂Cl₂ and MeOH, whereas the PF₆⁻ ion pair showed less solubility in the solvents that were available for **1au**⁺-FABA⁻.
- 14 K_{dim} of $\mathbf{1au}^+$ for $\mathbf{1au}^+$ -FABA $^-$ in DMSO- d_6 was estimated to be 400 M $^{-1}$.
- 15 Single crystals of **1au**⁺-FABA⁻ prepared from acetone/1,2-dichloroethane also afforded a similar packing structure.
- 16 Articles for GAMESS: (a) M. W. Schmidt, K. K. Baldridge, J. A. Boatz, S. T. Elbert, M. S. Gordon, J. H. Jensen, S. Koseki, N. Matsunaga, K. A. Nguyen, S. Su, T. L. Windus, M. Dupuis and J. A. Montgomery Jr, J. Comput. Chem., 1993, 14, 1347–1363; (b) M. S. Gordon and M. W. Schmidt, In Theory and Applications of Computational Chemistry: The First Forty Years ed. C. E. Dykstra, G. Frenking, K. S. Kim and G. E. Scuseria, Elsevier, 2005.
- 17 M. J. S. Phipps, T. Fox, C. S. Tautermann and C.-K. Skylaris, Chem. Soc. Rev., 2015, 44, 3177–3211.
- 18 Report for FMO: K. Kitaura, E. Ikeo, T. Asada, T. Nakano and M. Uebayasi, *Chem. Phys. Lett.*, 1999, 313, 701–706.
- 19 Report for pair interaction energy decomposition analysis (PIEDA): D. G. Fedorov and K. Kitaura, *J. Comput. Chem.*, 2007, **28**, 222–237.
- 20 (a) A. Acharya, S. Seki, A. Saeki, Y. Koizumi and S. Tagawa, *Chem. Phys. Lett.*, 2005, 404, 356–360; (b) S. Seki, A. Saeki, T. Sakurai and D. Sakamaki, *Phys. Chem. Chem. Phys.*, 2014, 16, 11093–11113.
- 21 Program and report for calculation of transfer integrals: (a) ADF (2024.1), SCM, Theoretical Chemistry, Vrije Universiteit, Amsterdam, 2024; (b) G. te Velde, F. M. Bickelhaupt, E. J. Baerends, C. Fonseca Guerra, S. J. A. van Gisbergen, J. G. Snijders and T. Ziegler, J. Comput. Chem., 2001, 22, 931–967.
- 22 T. Mori, A. Kobayashi, Y. Sasaki, H. Kobayashi, G. Saito and H. Inokuchi, *Bull. Chem. Soc. Jpn.*, 1984, 57, 627–633.
- 23 Hole transport can be acceptable in light of the electronic properties of $\mathbf{1au}^+$. Theoretical studies revealed a higher HOMO of $\mathbf{1au}^+$ than that of $\mathbf{2au}^+$, suggesting that π -expanded $\mathbf{1au}^+$, which is positively charged, would be suitable for hole transport (Fig. S35 and S40†). In addition,

- the HOMO of $1au^+$ is comparable to those of typical hole-transporting materials (ref. 1d).
- 24 Other precipitation conditions such as rapid precipitation using CH₃CN/CHCl₃ afforded crystalline precipitates with a packing structure similar to the single-crystal structure (Fig. S83†).
- 25 Small diffraction peaks would be derived from the unidentified packing structure of a minor species formed in the precipitation process.
- 26 The powder sample of **2au**⁺-FABA⁻ was prepared by precipitating from CH₂Cl₂/*n*-hexane.
- 27 K. Ohta, Physics and Chemistry of Molecular Assemblies, World Scientific, 2020.
- 28 Selected examples of liquid crystals and plastic crystals based on π-electronic molecules that have no aliphatic chains: (a) S. Basurto, S. García, A. G. Neo, T. Torroba, C. F. Marcos, D. Miguel, J. Barberá, M. B. Ros and M. R. de la Fuente, *Chem.-Eur. J.*, 2005, 11, 5362–5376; (b) D. Pucci, I. Aiello, A. Aprea, A. Bellusci, A. Crispini and M. Ghedini, *Chem. Commun.*, 2009, 1550–1552; (c) Y. Takagi, K. Ohta, S. Shimosugi, T. Fujii and E. Itoh, *J. Mater. Chem.*, 2012, 22, 14418–14425; (d) H. Nakamura, K. Sugiyama, K. Ohta and M. Yasutake, *J. Mater. Chem. C*, 2017, 5, 7297–7306; (e) K. Goossens, L. Rakers, B. Heinrich, G. Ahumada, T. Ichikawa, B. Donnio, T. J. Shin, C. W. Bielawski and F. Glorius, *Chem. Mater.*, 2019, 31, 9593–9603; (f) P. Guragain, M. Powers, J. Portman, B. Ellman and R. J. Twieg, *Mater. Adv.*, 2023, 4, 4129–4137.
- 29 B. Dario and G. Fabrizia, Chem. Soc. Rev., 2000, 29, 229-238.
- 30 The LeC states in this study might be considered as liquid crystals. The details will be discussed elsewhere.
- 31 M. Okazaki and C. A. McDowell, J. Am. Chem. Soc., 1984, 106, 3185–3190.
- 32 A. P. M. Kentgens, B. A. Markies, J. F. van der Pol and R. J. M. Nolte, *J. Am. Chem. Soc.*, 1990, **112**, 8800–8806.
- 33 Although the current evaluations for the bulk states suggest frozen-state properties at r.t. that are similar to those of single crystals, investigations according to thermal conditions would reveal more detailed information on dynamic thermal motion and less-ordered states.
- 34 Higher crystallinity compared to **1au**⁺-FABA⁻_P was suggested by the XRD analysis.
- 35 Ion-pairing assemblies in this study, exhibiting unconventional properties derived from charged π-electronic systems, are completely dissimilar from charge-transfer (CT) complexes that are obtained from electronically neutral donor and acceptor molecules. A review of CT complexes: M. Baharfar, A. C. Hillier and G. Mao, *Adv. Mater.*, 2024, **36**, 2406083.